Effective $J = 1/2$ Insulating State in Ruddlesden-Popper Iridates: An LDA + DMFT Study

Hongbin Zhang,* Kristjan Haule, and David Vanderbilt

Department of Physics and Astronomy, Rutgers University, Piscataway, New Jersey 08854, USA

(Received 20 August 2013; published 12 December 2013)

Using *ab initio* methods for correlated electrons in solids, we investigate the metal-insulator transition across the Ruddlesden-Popper (RP) series of iridates and explore the robustness of the $J_{\text{eff}} = 1/2$ state against band effects due to itineracy, tetragonal distortion, octahedral rotation, and Coulomb interaction. We predict the effects of epitaxial strain on the optical conductivity, magnetic moments, and $J_{\text{eff}} = 1/2$ ground-state wave functions in the RP series. To describe the solution of the many-body problem in an intuitive picture, we introduce a concept of energy-dependent atomic states, which strongly resemble the atomic $J_{\text{eff}} = 1/2$ states but with coefficients that are energy or time dependent. We demonstrate that the deviation from the ideal $J_{\text{eff}} = 1/2$ state is negligible at short time scales for both single- and double-layer iridates, while it becomes quite significant for $Sr_3Ir_2O_7$ at long times and low energy. Interestingly, Sr_2IrO_4 is positioned very close to the $SU(2)$ limit, with only ~3% deviation from the ideal $J_{\text{eff}} = 1/2$ situation.

DOI: 10.1103/PhysRevLett.111.246402 PACS numbers: 71.30.+h, 71.15.−m, 71.20.−b

Metal-insulator transitions are very common in $3d$ transition-metal oxides due to the small bandwidth of the $3d$ orbitals and the poorly screened electron-electron interaction on the $3d$ ions [1]. Because of the larger spatial extent of the $5d$ orbitals, the $5d$ transition-metal oxides are expected to be more itinerant. However, because of strong spin-orbit coupling (SOC), many $5d$ transition-metal oxides show significant electron-electron correlations and even metal-insulator transitions of possible Mott type. One of the most well-studied $5d$ systems at the localization-delocalization boundary is the Ruddlesden-Popper (RP) series of iridates with chemical formula $Sr_{n+1}Ir_nO_{3n+1}$, where n is the number of $SrIrO_3$ perovskite layers sandwiched between extra SrO layers.

Experimentally, Sr_2IrO_4 (214) is a Mott-like magnetic insulator with canted in-plane antiferromagnetic (AFM) ordering [2–5], $Sr_3Ir_2O_7$ (327) is a narrow-gap AFM insulator in proximity to a metal-insulator transition [5] with moments aligned along the c axis [6,7], and $SrIrO_3$ (113) is a correlated metal [8].

These compounds have attracted tremendous attention recently [9–11] because of the similarity between 214 and the parent compound La_2CuO_4 of the cuprate superconductors: the structures are the same, the low-energy properties can be modeled by a single band Hubbard-type model [9], and the magnetic spin-wave spectrum in Sr_2IrO_4 shows no observable spin-wave gap [12]. This is quite unexpected because the large SOC and IrO_6 octahedral rotations lead to significant Dzyaloshinsky-Moriya interaction. On the other hand, a very different spin-wave spectrum with a large magnon gap was found in the double-layer 327 compound [13].

Kim *et al.* [9] proposed that the strong SOC and the large octahedral crystal-field splitting between the t_{2g} and e_g states produce an effective $J_{\text{eff}} = 1/2$ state on the Ir^{4+} ion, where the magnetic moment is isotropic and $SU(2)$ invariant. In the following, the point of vanishing magnetic anisotropy is called the $SU(2)$ point. The $J_{\text{eff}} = 1/2$ states form a Kramers doublet and contain an equal mixture of d_{xz}, d_{yz}, and d_{xy} orbitals in the form $|\psi_{-1/2}\rangle = (|d_{xy}\uparrow\rangle + |d_{yz}\downarrow\rangle + i|d_{xz}\downarrow\rangle)/\sqrt{3}$ and $|\psi_{+1/2}\rangle = (-|d_{xy}\downarrow\rangle + |d_{yz}\uparrow\rangle - i|d_{xz}\uparrow\rangle)/\sqrt{3}$. This is the ground state of a single ion in a cubic crystal environment, which carries a magnetic moment of $1\mu_B$. Experimentally, the Ir ions in 214 have significantly smaller sublattice magnetic moments of the order of $0.5\mu_B$ [2], which demonstrates the importance of itineracy in this system. Moreover, the tetragonal distortions in all members of the RP series of iridates are large, leading to a crystal-field splitting $\Lambda \equiv \varepsilon_{xz} - \varepsilon_{xy}$ between d_{xy} and $d_{xz/yz}$ orbitals that breaks the $SU(2)$ invariance of the magnetic moments. Nevertheless, the absence of resonant x-ray magnetic scattering intensity at the L_2 edge suggests that the electronic state in both the single-layer [3] and double-layer [14] members of the RP series are quite close to the $J_{\text{eff}} = 1/2$ limit.

In this Letter, we have performed dynamical mean field theory (DMFT) calculations [15] in a charge self-consistent implementation [16] on top of density functional theory (DFT), allowing for a realistic treatment of competing crystal-field, SOC, and Coulomb interaction (for details, see the Supplemental Material [17]). In particular, the explicit inclusion of ligand states, which goes beyond previous DMFT studies of this class of materials [18,19], was crucial for a correct description of the dynamic crystal-field effects. Our work provides quantitative answers to the questions of how good is the $J_{\text{eff}} = 1/2$ description in the RP series of iridates, and how large is the deviation from the isotropic $SU(2)$ magnetic response. We show that the answers to these questions have a time-scale or

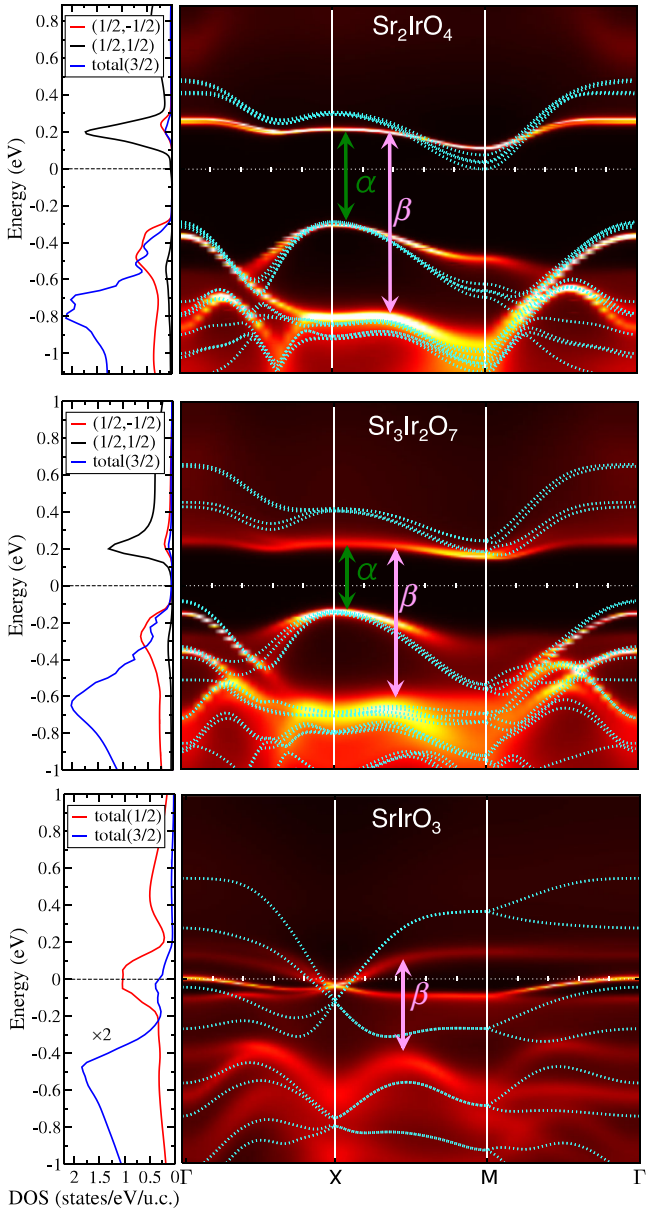

FIG. 1 (color online). Spectral functions and orbital-resolved DOS obtained by the DMFT method for the RP series of iridates. Arrows indicate optical transitions corresponding to the peaks in the optical conductivities shown in Fig. 2. Dotted lines denote the band structures obtained by GGA + U calculations. For 214 and 327, the GGA + U band structures and the DMFT spectral functions are aligned by fixing the position of the topmost valence state at X. Orbitals $(1/2, \pm 1/2)$ correspond to $\psi_{\pm 1/2}$, and "total(3/2)" stands for the sum over the remaining t_{2g} states, i.e., $J_{\mathrm{eff}} = 3/2$ states.

energy-scale dependence, thus, resolving some points of controversy in the literature.

Our DFT + DMFT calculations are done using the projection-embedding implementation [16] based on the WIEN2K package [20]. For comparison, we also carried out DFT + U calculations using the ELK code [21]. VASP was used to relax the structures when epitaxial strain was considered [22]. Details are provided in the Supplemental Material [17].

The resulting DMFT spectral functions are presented in Fig. 1 for the 214, 327, and 113 compounds, with color coding showing the spectral intensity along $\Gamma - X - M - \Gamma$, together with orbital-resolved density of states (DOS) band structures obtained using generalized gradient approximation + U (GGA + U). Within DMFT, the insulating gap in 214 and 327 are approximately 400 and 300 meV, respectively. The unoccupied electronic states are of mainly $J_{\mathrm{eff}} = 1/2$ character. The first valence state at X is also of $J_{\mathrm{eff}} = 1/2$ character, while the first valence state at Γ is of $J_{\mathrm{eff}} = 3/2$ character; hence, the occupied states are an equal mixture of $J_{\mathrm{eff}} = 1/2$ and $J_{\mathrm{eff}} = 3/2$ states. In the DMFT calculation, the topmost valence state at X is about 40 meV closer to E_F than the first valence state at the Γ point, in agreement with recent angle-resolved photoemission spectroscopy (ARPES) measurements [23,24] but in contrast to GGA + U results (Fig. 1). This is because the filled orbitals (here, $J_{\mathrm{eff}} = 3/2$) tend to be repelled from the Fermi level in DMFT. In 327, the $J_{\mathrm{eff}} = 3/2$ tail at Γ is split into two peaks due to its double-layer structure, consistent with experimental results [25]. Finally, the 113 compound is a strongly correlated metal [8] with very flat bands around E_F. The effective mass of the t_{2g} states is quite large; e.g., the effective mass of the hole pocket around Γ is about 9 times that of a bare electron.

A closer look at the orbital-resolved DOS in Fig. 1 reveals that the $J_{\mathrm{eff}} = 1/2$ states are not fully polarized. This is due to significant itineracy effects and hybridization between Ir $5d$ and O $2p$ states. The resulting occupation number for the occupied $J_{\mathrm{eff}} = 1/2$ orbitals is about 0.65 (0.45) in the 214 (327) compound. Consequently, this leads to substantially reduced magnetic moments compared to the ideal $J_{\mathrm{eff}} = 1/2$ value of $1\mu_B$, down to about 0.55 (214) and $0.58\mu_B$ (327).

While for the most part, the GGA + U band structures are in fairly good agreement with the DMFT spectral functions (Fig. 1), there are also some differences. The band gaps in the 214 and 327 compounds within GGA + U are of almost equal size, about 270 meV ($U_{\mathrm{GGA+U}} = 2.5$ eV), while there is a clear gap reduction of about 100 meV in the DMFT calculations. This is not surprising, given that the fully screened U required by GGA + U should be reduced in the more itinerant 327 compounds. For 113, the Fermi surfaces in DMFT are quite similar to the GGA Fermi surfaces (not shown), but the bandwidth is strongly renormalized. This is not the case in GGA + U, where the hole pocket at Γ is missing. Recent ARPES measurements [26] confirmed the existence of the hole pocket at Γ with a strongly enhanced effective mass, in agreement with our DMFT results.

We mention in passing that the paramagnetic calculation for 214 is not insulating in DFT + DMFT, but a very bad

metal, in agreement with the DMFT calculations of Ref. [18], but in disagreement with Ref. [19], where the Mott gap was found in the absence of long- or short-range order, placing the material into the strong coupling regime. The single-site DMFT calculations describe the correlations local to the Ir sites exactly, and infinite-range correlations in a mean-field way, when AFM ordering is imposed. Fujiyama *et al.* [4] reported a large but finite correlation length exceeding 100 lattice spacings even 20 K above the Néel temperature in 214. The "marginal Mott insulator" [4], a term coined to describe such a short-range-ordered state, is not captured by the single-site DMFT method but requires cluster extensions. We also note that the temperature dependence of the optical conductivity of Ref. [27] is not consistent with the strong coupling regime, as defined in Ref. [28], but it is more consistent with the intermediate coupling, as the optical weight is roughly temperature independent when integrated up to 1.5 eV.

The optical conductivities for the three compounds obtained by the DMFT calculations are shown in Fig. 2. In agreement with experiments [29], the optical conductivities of the 214 and 327 insulating compounds have two peaks denoted by α and β in the low-energy range (0–1.2 eV). As proposed in Ref. [27], the α peak is mainly due to the excitations from the highest valence band to the first conduction band, both being of primarily $J_{\rm eff} = 1/2$ character. The second peak is mainly due to the excitations from the lower valence bands, of primarily $J_{\rm eff} = 3/2$ character, to the conduction band of $J_{\rm eff} = 1/2$ character. It is interesting to note that even though there is no clear separation in energy between $J_{\rm eff} = 1/2$ and $J_{\rm eff} = 3/2$ valence states (Fig. 1), the vertical excitations probed by optics do give rise to two well-separated peaks. Going from

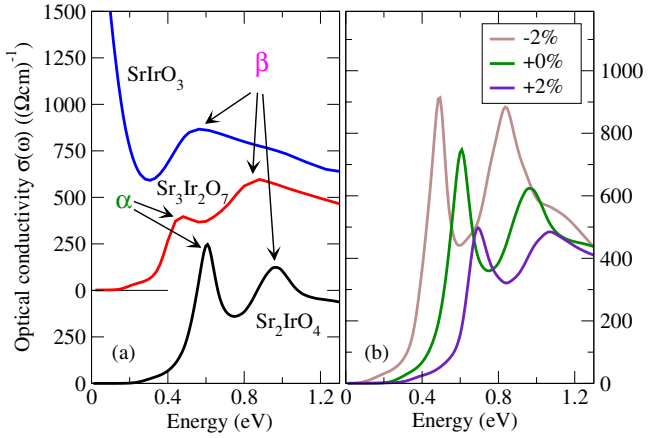

FIG. 2 (color online). (a) Computed optical conductivities σ_1 for three iridates at their experimental lattice constants. For clarity, σ_1 is shifted up by 500 $(\Omega\,\mathrm{cm})^{-1}$ for $Sr_3Ir_2O_7$ and $SrIrO_3$; α and β indicate peak positions corresponding to the vertical transitions marked in Fig. 1. (b) Dependence of σ_1 on epitaxial strain (0% and ±2%) in Sr_2IrO_4.

214 to 327, the α peak shifts by about 100 meV to lower energy, while it is replaced by a narrow Drude peak in the 113 compound. The β peak broadens and shifts from 1.0 eV in 214 to 0.5 eV in 113, in good agreement with experiments [29]. We notice that there is an observable tail of optical conductivity, as also found in optical measurements [27,29], for both insulating compounds at low energy (spanning the region from 0.25 eV to about 0.4 eV in 214), which can be attributed to the incoherent spectral weight in the gap.

To shed more light on the nature of the $J_{\rm eff} = 1/2$ insulating state, we performed calculations for the RP series of iridates under epitaxial strain. The evolution of the structural parameters under epitaxial strain is shown in Fig. 3. Both the c/a ratio, panels 3(c) and 3(f), and the rotation angle θ of the IrO_6 octahedra, panels 3(b) and 3(e), decrease nearly linearly with increasing in-plane lattice constants, in quantitative agreement with recent experiments [30]. Figure 2(b) shows the optical conductivity for 214 with −2% (compressive), 0%, and +2% (tensile) strain. Compressive (tensile) strain substantially reduces (increases) the gap size due to an increase (decrease) of the

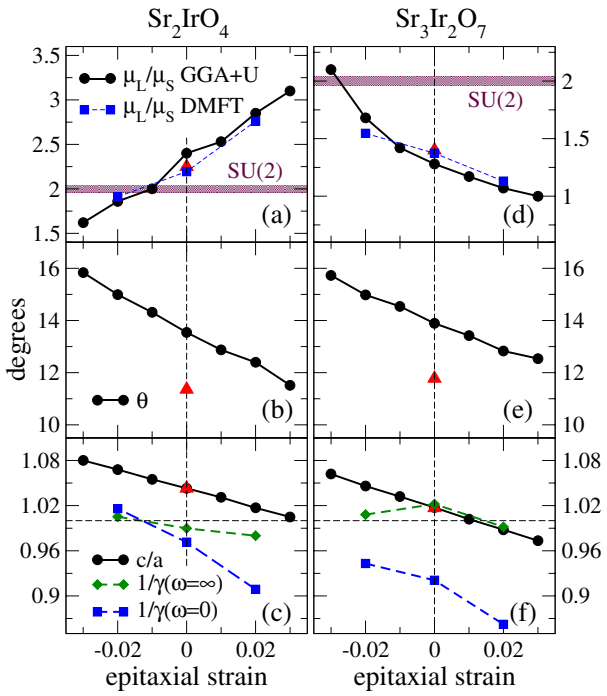

FIG. 3 (color online). Dependence of computed properties of the 214 (a)–(c) and 327 (d)–(f) compounds on epitaxial strain in the range of ±3%. (a),(d) Orbital-to-spin moment ratio μ_L/μ_S. (b),(e) Staggered rotation angle θ of IrO_6 octahedra. (c),(f) Ratio of Ir-O bond lengths along z and in-plane c/a, and inverse of parameter γ describing the generalized $J_{\rm eff} = 1/2$ wave function (see main text). Filled symbols with dashed (solid black) lines denote the results obtained by DMFT (GGA + U) calculations. Red triangles indicate GGA + U results computed with unrelaxed experimental lattice parameters.

dominant in-plane hoppings. The two peaks are shifted to lower (higher) energy and become sharper (broadened), while the overall conductivity increases (decreases) under compressive (tensile) strain. This is in good agreement with recent optical measurements on strained 214 thin films [30].

For the ideal $J_{\mathrm{eff}} = 1/2$ state, the orbital magnetic moment of the Ir atoms is twice as large as the spin moment, with values of 2/3 and 1/3 μ_B, respectively. Figures 3(a) and 3(d) show the $\mu_{\mathrm{L}}/\mu_{\mathrm{S}}$ ratio as obtained by the DMFT and GGA + U methods for the 214 and 327 compounds. In 214, this ratio increases with tensile strain, while it decreases in 327. In the absence of strain, $\mu_{\mathrm{L}}/\mu_{\mathrm{S}} \approx 2.2$ for 214 and $\mu_{\mathrm{L}}/\mu_{\mathrm{S}} \approx 1.3$ for 327, which demonstrates that 214 has only a slightly larger orbital moment than expected for the ideal $SU(2)$ situation [31], while 327 has a substantially smaller orbital moment. For the 214 (327) compounds, the $SU(2)$ point can be reached by 1% (3%) compressive strain. It is interesting to note that at this $SU(2)$ point, the IrO_6 octahedra are significantly elongated in the z direction ($c/a \approx 1.05$). Thus, the deviation from $SU(2)$ behavior is not simply associated with tetragonality, as might have been expected.

To gain some understanding into this puzzling behavior, we analyzed the DMFT hybridization function $\Delta(\omega)$, which carries all the information about the crystal environment for an electron on a given iridium site. It is defined by $1/(\omega - \Delta - \Sigma) = \sum_k \hat{P}/(\omega + \mu - \varepsilon_k - \hat{P}^{-1}\Sigma)$. Here, Σ is the DMFT self-energy, ε_k are the Kohn-Sham-like eigenvalues, and $\hat{P}$ ($\hat{P}^{-1}$) is the projector (embedder) on the Ir site. In the high-frequency limit, $\Delta(\omega \to \infty) = \sum_k \hat{P}(\varepsilon_k - \mu)$ is a matrix whose elements denote the atomic on-site energy levels. It includes both the crystal-field and SOC terms, and it is directly related to the so-called single-ion anisotropy. The low-energy counterpart $\Delta(\omega = 0)$ is related to the low-energy excitations such as spin waves.

For both 214 and 327, the hybridization function can be well represented by the matrix

$$\Delta(\omega) = \begin{pmatrix} & xz\uparrow & yz\uparrow & xy\downarrow \\ xz\uparrow & \epsilon & -i(\lambda/2) & i[(\lambda/2)+\delta] \\ yz\uparrow & i(\lambda/2) & \epsilon & -[(\lambda/2)+\delta] \\ xy\downarrow & -i[(\lambda/2)+\delta] & -[(\lambda/2)+\delta] & \epsilon - \Lambda \end{pmatrix}, \tag{1}$$

where ϵ indicates the on-site energy, λ the SOC strength, Λ the $d_{xz/yz}/d_{xy}$ crystal-field splitting, and δ the renormalization of the SOC between the d_{xy} and $d_{xz/yz}$ orbitals. In general, all of these parameters are frequency dependent. For the above matrix, the largest eigenvalue corresponds to eigenvectors

$$|\psi_{+(1/2)}\rangle = -\sqrt{\frac{3-2\gamma(\omega)^2}{3}}|d_{xy}\downarrow\rangle + \frac{\gamma(\omega)}{\sqrt{3}}(|d_{yz}\uparrow\rangle - i|d_{xz}\uparrow\rangle),$$
$$|\psi_{-(1/2)}\rangle = \sqrt{\frac{3-2\gamma(\omega)^2}{3}}|d_{xy}\uparrow\rangle + \frac{\gamma(\omega)}{\sqrt{3}}(|d_{yz}\downarrow\rangle + i|d_{xz}\downarrow\rangle). \tag{2}$$

This is a generalization of the ideal $J_{\mathrm{eff}} = 1/2$ wave function, which is recovered when $\gamma = 1$. For small deviation from the ideal $SU(2)$ case ($\Lambda/\lambda \ll 1$ and $\delta/\lambda \ll 1$), one finds $\gamma = 1 + \frac{2}{9}(\Lambda - \delta/\lambda) + \cdots = 1 + \tilde{\gamma}$, where $\tilde{\gamma} \equiv \gamma - 1$ is a small deviation of positive or negative sign for $J_{\mathrm{eff}} = 1/2$ states that are, respectively, expanded or contracted in the z direction.

The values of $1/\gamma(\omega = \infty)$ and $1/\gamma(\omega = 0)$, as obtained by exact diagonalization of the hybridization matrix, are plotted in Figs. 3(c) and 3(f). In a simplified model, where only splitting between d_{xy} and $d_{yz/xz}$ due to the tetragonal distortion of IrO_6 octahedra is considered, $1/\gamma$ is expected to be directly proportional to the c/a ratio and $1/\gamma = 1.0$ when $c/a = 1$. Clearly, this is not the case as shown in Figs. 3(c) and 3(f). In the high-frequency limit, $\gamma(\omega = \infty)$ deviates from the ideal value of unity by less than 2%, which shows that the single-ion anisotropy is small in both compounds. In the low-frequency limit, which is more relevant for spin dynamics, we can approximate $\gamma(\omega = 0) \approx 1.03 + 3.5r$ in 214, where r denotes the amount of epitaxial strain. In the absence of strain, this is quite close to unity and reaches the ideal value upon 0.9% compressive strain ($r = -0.009$). The behavior in 327 is quite different, where $\gamma(\omega = 0) \approx 1.08 + 2.5r$. A substantial deviation of 8% from the $SU(2)$ value is obtained in the absence of strain, and more than 3% compressive strain is required to recover an isotropic magnetic moment.

Our *ab initio* values of $\mu_{\mathrm{L}}/\mu_{\mathrm{S}}$ are well accounted for by this simplified model when $\gamma(\omega = 0)$ is used. In 214, the magnetic moments are ordered in plane, so that $\mu_{\mathrm{L}}^{xy}/\mu_{\mathrm{S}}^{xy} \approx (\frac{2}{3} - \frac{2}{3}\tilde{\gamma})/(\frac{1}{3} - \frac{4}{3}\tilde{\gamma}) \approx 2 + 6\tilde{\gamma} \approx 2.2 + 21r$ (see the Supplemental Material [17] for details), which is quite close to the *ab initio* calculated line in Fig. 3(a). In 327, the AFM moments are ordered in the z direction, hence, $\mu_{\mathrm{L}}^{z}/\mu_{\mathrm{S}}^{z} \approx (\frac{2}{3} + \frac{4}{3}\tilde{\gamma})/(\frac{1}{3} + \frac{8}{3}\tilde{\gamma}) \approx 2 - 12\tilde{\gamma} \approx 1.04 - 30r$. Because of the much larger deviation $\tilde{\gamma}$, this approximation is not very accurate, but it nevertheless gives a decreasing moment ratio $\mu_{\mathrm{L}}/\mu_{\mathrm{S}}$ with tensile strain and a large deviation of this ratio from the ideal $SU(2)$ value of 2.

Finally, let us comment on the *ab initio* values of the entries in the hybridization matrix, Eq. (1). At high frequency $\Delta(\omega \to \infty)$, the crystal-field splitting is typically only $\Lambda \approx 25$ meV, while the SOC strength $\lambda/2 \approx 250$ meV, and the SOC enhancement δ vanishes. This gives $\gamma(\omega = \infty) \approx 1.01$, as shown in Figs. 3(d) and 3(h). At low energy, the crystal-field splitting is strongly enhanced by the hybridization effects of the tetragonal crystal structure. In 214, it typically takes a value of

$\Lambda \approx 140$ meV. Unexpectedly, δ is of similar magnitude; hence, $\gamma(\omega = 0) \approx 1 + \frac{2}{9}(\Lambda - \delta)/\lambda$ is again close to unity. In 327, the enhancement of crystal fields is even larger ($\Lambda \approx 300$ meV), but δ is somewhat smaller ($\delta \approx 120$ meV) compared to that in 214, resulting in the 8% deviation of γ from the ideal value. We note that the proximity to the $SU(2)$-invariant point leads to isotropic moments and almost gapless spin-wave excitations, which is in qualitative agreement with recent measurements where a small spin gap was found in 214 [12] and a large spin gap in 327 [13].

In summary, our simulations demonstrate the fragile nature of the $J_{\text{eff}} = 1/2$ state in iridates and show that Sr_2IrO_4 is positioned close to the ideal $J_{\text{eff}} = 1/2$ point while $Sr_3Ir_2O_7$ is farther away. The deviation from this special $SU(2)$ point is smaller at short times because it is controlled by the instantaneous crystal-field splitting, while it is enhanced at long times due to hybridization-driven crystal-field effects that are rooted in the strong hybridization between Ir d and oxygen p states.

We acknowledge insightful discussions with George Jackeli, Kyle Shen, and Jaejun Yu. This work was supported by NSF Grant No. DMREF-12-33349.

*Corresponding author.
hzhang@physics.rutgers.edu

[1] M. Imada, A. Fujimori, and Y. Tokura, Rev. Mod. Phys. **70**, 1039 (1998).
[2] G. Cao, J. Bolivar, S. McCall, J. E. Crow, and R. P. Guertin, Phys. Rev. B **57**, R11039 (1998).
[3] B. J. Kim, H. Ohsumi, T. Komesu, S. Sakai, T. Morita, H. Takagi, and T. Arima, Science **323**, 1329 (2009).
[4] S. Fujiyama, H. Ohsumi, T. Komesu, J. Matsuno, B. J. Kim, M. Takata, T. Arima, and H. Takagi, Phys. Rev. Lett. **108**, 247212 (2012).
[5] D. A. Zocco, J. J. Hamlin, B. J. Kim, J. R. Jeffries, S. T. Weir, Y. K. Vohra, J. W. Allen, and M. B. Maple, arXiv:1304.5864.
[6] G. Cao, Y. Xin, C. S. Alexander, J. E. Crow, P. Schlottmann, M. K. Crawford, R. L. Harlow, and W. Marshall, Phys. Rev. B **66**, 214412 (2002).
[7] S. Fujiyama, K. Ohashi, H. Ohsumi, K. Sugimoto, T. Takayama, T. Komesu, M. Takata, T. Arima, and H. Takagi, Phys. Rev. B **86**, 174414 (2012).
[8] G. Cao, V. Duarairaj, S. Chikara, L. E. DeLong, S. Parkin, and P. Schlottmann, Phys. Rev. B **76**, 100402 (2007).
[9] B. J. Kim, H. Jin, S. J. Moon, J.-Y. Kim, B.-G. Park, C. S. Leem, J. Yu, T. W. Noh, C. Kim, S.-J. Oh, J.-H. Park, V. Durairaj, G. Cao, and E. Rotenberg, Phys. Rev. Lett. **101**, 076402 (2008).
[10] G. Jackeli and G. Khaliullin, Phys. Rev. Lett. **102**, 017205 (2009).
[11] F. Wang and T. Senthil, Phys. Rev. Lett. **106**, 136402 (2011).
[12] J. Kim, D. Casa, M. H. Upton, T. Gog, Y.-J. Kim, J. F. Mitchell, M. van Veenendaal, M. Daghofer, J. van den Brink, G. Khaliullin, and B. J. Kim, Phys. Rev. Lett. **108**, 177003 (2012).
[13] J. Kim, A. H. Said, D. Casa, M. H. Upton, T. Gog, M. Daghofer, G. Jackeli, J. van den Brink, G. Khaliullin, and B. J. Kim, Phys. Rev. Lett. **109**, 157402 (2012).
[14] S. Boseggia, R. Springell, H. C. Walker, A. T. Boothroyd, D. Prabhakaran, D. Wermeille, L. Bouchenoire, S. P. Collins, and D. F. McMorrow, Phys. Rev. B **85**, 184432 (2012).
[15] G. Kotliar, S. Y. Savrasov, K. Haule, V. S. Oudovenko, O. Parcollet, and C. A. Marianetti, Rev. Mod. Phys. **78**, 865 (2006).
[16] K. Haule, C.-H. Yee, and K. Kim, Phys. Rev. B **81**, 195107 (2010).
[17] See Supplemental Material at http://link.aps.org/supplemental/10.1103/PhysRevLett.111.246402 for computation details, derivation of magnetic moments, and detailed analysis of the electronic structures.
[18] R. Arita, J. Kunes, A. V. Kozhevnikov, A. G. Eguiluz, and M. Imada, Phys. Rev. Lett. **108**, 086403 (2012).
[19] C. Martins, M. Aichhorn, L. Vaugier, and S. Biermann, Phys. Rev. Lett. **107**, 266404 (2011).
[20] http://www.wien2k.at.
[21] http://elk.sourceforge.net.
[22] http://www.vasp.at.
[23] B. M. Wojek, M. H. Berntsen, S. Boseggia, A. T. Boothroyd, D. F. McMorrow, H. M. Rønnow, J. Chang, and O. Tjernberg, J. Phys. Condens. Matter **24**, 415602 (2012).
[24] Q. Wang, Y. Cao, J. A. Waugh, S. R. Park, T. F. Qi, O. B. Korneta, G. Cao, and D. S. Dessau, Phys. Rev. B **87**, 245109 (2013).
[25] P. D. C. King, T. Takayama, A. Tamai, E. Rozbicki, S. M. Walker, M. Shi, L. Patthey, R. G. Moore, D. Lu, K. M. Shen, H. Takagi, and F. Baumberger, Phys. Rev. B **87**, 241106 (2013).
[26] Y. Nie, P. D. C. King, and K. M. Shen (private communication).
[27] S. J. Moon, H. Jin, W. S. Choi, J. S. Lee, S. S. A. Seo, J. Yu, G. Cao, T. W. Noh, and Y. S. Lee, Phys. Rev. B **80**, 195110 (2009).
[28] C. Taranto, G. Sangiovanni, K. Held, M. Capone, A. Georges, and A. Toschi, Phys. Rev. B **85**, 085124 (2012).
[29] S. J. Moon, H. Jin, K. W. Kim, W. S. Choi, Y. S. Lee, J. Yu *et al.*, Phys. Rev. Lett. **101**, 226402 (2008).
[30] J. Nichols, J. Terzic, E. G. Bittle, O. B. Korneta, L. E. De Long, J. W. Brill, G. Cao, and S. S. A. Seo, Appl. Phys. Lett. **102**, 141908 (2013).
[31] While this Letter was in preparation, we became aware of work by Fujiyama *et al.* [32] where the ratio μ_L/μ_S of 214 was estimated to be 2.5 ± 0.35 by nonresonant magnetic x-ray scattering (NRMXS) measurements, close to our theoretical value of $\mu_L/\mu_S \approx 2.2$.
[32] S. Fujiyama, H. Ohsumi, K. Ohashi, D. Hirai, B. J. Kim, T. Arima, M. Takata, and H. Takagi, arXiv:1308.0923.